*Journal of Low Temperature Physics, Vol. 139, Nos. 3/4, May 2005 (© 2005)*
DOI: 10.1007/s10909-005-4730-5

# Cavitation of Electron Bubbles in Liquid Helium Below Saturation Pressure

**Martí Pi, Manuel Barranco, Ricardo Mayol, and Víctor Grau**

*Departament ECM, Facultat de Física, Universitat de Barcelona, E-08028 Barcelona, Spain*

(Received September 16, 2004; revised February 4, 2005)

*We have used a Hartree–type electron–helium (e–He) potential together with a density functional description of liquid $^4He$ and $^3He$ to study the explosion of electron bubbles submitted to a negative pressure. The critical pressure at which bubbles explode has been determined as a function of temperature. It has been found that this critical pressure is very close to the pressure at which liquid helium becomes globally unstable in the presence of electrons. It is shown that at high temperatures the capillary model overestimates the critical pressures. We have checked that a commonly used and rather simple e-He interaction yields results very similar to those obtained using the more accurate Hartree-type interaction. We have estimated that the crossover temperature for thermal to quantum nucleation of electron bubbles is very low, of the order of 6 mK for $^4He$.*

***KEY WORDS*:** cavitation; electron bubbles; liquid helium.

## 1. INTRODUCTION

It has been recognized that liquid helium is especially well suited for homogeneous cavitation studies. On the one hand, it can be prepared in a high-purity state, avoiding heterogeneous cavitation driven by impurities in the liquid. Besides, experimental techniques have been developed[1–4] that focus a short burst of ultrasound into a small volume of bulk liquid, thus preventing cavitation on defects at the walls of the experimental cell. On the other hand, helium remains liquid down to zero temperature ($T$). This allows to address quantum cavitation, a phenomenon that may appear at very low temperatures.[3,5,6]

Heterogeneous cavitation produced by impurities purposely introduced in the liquid is also interesting by itself,[7] and in a series of recent



0022-2291/05/0500-0397/0 

experiments the case of heterogeneous cavitation caused by electrons (electron bubble explosions) has been addressed in detail.[8–10] Another interesting case of heterogeneous cavitation in liquid $^4$He thoroughly studied is that caused by the presence of quantized vortices acting as cavitation seeds.[11–13]

In this work we attempt a theoretical description of electron bubble explosions using a $T$-dependent density functional approach we have employed in a series of studies on cavitation and nucleation in liquid helium (see Ref. 14 for a comprehensive review) in conjunction with a realistic electron–helium (e–He) effective potential. Our results are in agreement with those obtained in Refs. 8 and 9 for $^4$He, and in Ref. 10 for $^3$He, covering a wider temperature range.

This paper is organized as follows. Sections 2 and 3 are mostly devoted to $^4$He and to the general formalism. In Sec. 2 we present the results obtained using the capillary approximation. In the case of electron bubbles, this approximation has been considered realistic enough to yield semi-quantitative results for critical pressures and thermal to quantum crossover temperatures, and constitutes a useful guide to the results obtained within density functional (DF) theory. In Sec. 3 we present the DF plus Hartree electron-effective potential approach together with the results obtained for $^4$He using this method. In Sec. 4 we present the results obtained for $^3$He, and a brief summary is presented in Sec. 5. A preliminary version of part of this work has been presented elsewhere.[15]

## 2. CAPILLARY MODEL

In this simple model, the electron is confined in an impenetrable spherical well potential of radius $R$. The total energy of the e–He system can be written as a function of the radius as[16,17]

$$U(R) = \frac{\pi^2\hbar^2}{2m_e R^2} + 4\pi R^2\sigma + \frac{4}{3}\pi R^2 P - \xi\frac{\epsilon-1}{\epsilon}\frac{e^2}{2R}, \tag{1}$$

where $P$ is the pressure applied to the system, $\sigma$ is the surface tension of the liquid, and $\epsilon$ is its dielectric constant. The first term is the energy of the electron in the ground-state of an infinite well potential of radius $R$. For $^4$He the last term can be evaluated taking $\epsilon = 1.0588$ (Ref. 18) and $\xi = 1.345$ (Ref. 17). Its effect is small and it will not be considered in the following. We have also checked that the effect of including a curvature energy term in Eq.(1) is small. On the contrary, the effect of the surface tension on any cavitation process is crucial, and quantitative results can only be obtained with the use of the correct value of $\sigma$. In the following, we will take[19] $\sigma = 0.272\,\mathrm{K\,\AA^{-2}}$, instead of the value $\sigma = 0.257\,\mathrm{K\,\AA^{-2}}$

given in Ref 20 that we and other authors have used in the past.[8,9,13,21] We want to mention that the value of Roche *et al.*[19] agrees well with that of Guo *et al.*[22] obtained long time ago.

When $P \geqslant 0$ Eq. (1) has an absolute minimum located at $R_{\min} = 18.9\,\text{Å}$ at $P = 0$. This configuration corresponds to a stable electron bubble. When the liquid is depressed below its saturation vapor pressure, the absolute minimum becomes local, and $U(R)$ also displays a local maximum. The metastability region in the $P - T$ plane extends between the liquid–vapor coexistence line down to the instability line. Consequently, metastable bubbles can be formed at positive and negative pressures as well. In that region, the electron bubbles are metastable, and an energy barrier of height $\triangle U = U(R_{\max}) - U(R_{\min})$ appears which can be overcome either by thermal activation above the barrier or by quantum tunnelling through it.

The height of the energy barrier $\triangle U$ is displayed in Fig. 1 as a function of $P$ at $T = 0\,\text{K}$. It can be seen that if the negative pressure is large enough, the barrier eventually disappears and the system becomes globally unstable. This happens at an instability pressure $P_u$ given by the expression:

$$P_u = -\frac{16}{5}\left(\frac{2\pi m_e}{5\hbar^2}\right)^{1/4}\sigma^{5/4}. \tag{2}$$

For the parameters we use, $P_u = -2.12$ bar, and the radius of the corresponding electron bubble is $R_u = 28.2\,\text{Å}$. Had we taken into account the last term in Eq. (1), we would have obtained $P_u = -2.24$ bar and $R_u = 27.1\,\text{Å}$. The instability pressure can be compared to the spinodal pressure at which pure $^4$He liquid becomes macroscopically unstable, $P_{sp} = -9.20\,\text{bar}$.[21] This value of $P_{sp}$ is consistent with the value obtained by other authors.[9,23,24]

A necessary condition for the validity of the capillary model is that the metastable electron bubble has a fairly large radius. Only in this case one may split the system into a volume and a surface region which justifies the use of Eq. (1). This happens when the critical configurations are large enough, as for example in the case of cavitation occuring near the liquid-vapor coexistence line.[23,25] However, in the case of electron bubble explosions the situation is more complex because the e–He interaction is strongly repulsive and small changes in the electron wave function may cause a sizeable effect on the metastable bubble. It is obvious that the bubble configurations used in the capillary model have little flexibility, and consequently, the validity of this approximation should eventually rely on the comparison with more realistic methods, as the DF approach. This will be done in Sec. 3.

In most cases, cavitating liquids undergo phase separation before they reach the stage of global unstability. This proceeds through the formation

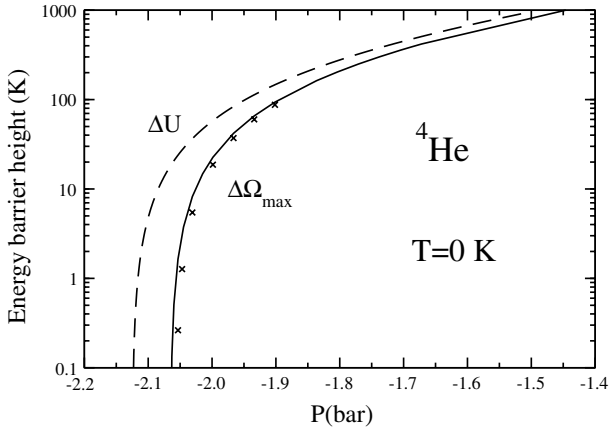


Fig. 1. Energy barrier height $\triangle U$ (K) (dashed line) as a function of $P$ (bar) of an electron bubble in liquid $^4$He at $T = 0$ in the capillary model. Also shown is the corresponding DF result (solid line). The crosses along the DF curve have been obtained using a simpler electron–He interaction, see text.

of critical bubbles either by thermal or by quantum activation. We will show that for electron bubbles, the critical pressure $P_{cr}$ at which it happens is very close to $P_u$, a result already obtained in Ref. 9. As a general rule, the presence of impurities in the liquid results in a sizeable decrease of $|P_{cr}|$. Quantized vortices in liquid $^4$He play the same role as impurities, and their presence also decrease $|P_{cr}|$ (Refs. 11 and 12) as well as the degree of critical supersaturation in $^3$He–$^4$He liquid mixtures.[13]

Within the capillary approximation, the dynamical evolution of the electron bubble can be parametrized by one single collective variable, namely the radius of the bubble. In this case, it is rather simple to describe quantum and thermal cavitation regimes on the same footing, continuously passing from one to the other. This is accomplished by the use of the functional integral method (FIM)[26,27] thoroughly described in Ref. 13. We now recall its essentials.

The nucleation rate $J$ for a thermally activated process, i.e., the number of critical bubbles formed in the system per unit time and volume, is

$$J_T = J_{0T} \exp(-\Delta U / k_B T), \tag{3}$$

where $k_B$ is the Boltzmann constant. The prefactor $J_{0T}$ depends on the dynamics of the process, and it is of the order of the number of cavitation. sites per unit volume (the number of electrons per unit volume, $n_e$ in the

present case) times an attempt frequency $\nu_T$. For simplicity, we take $\nu_T = k_B T/h$, where $h$ is the Planck constant.

At low enough $T$, thermal activation is no longer possible. However, cavitation may proceed by quantum tunnelling. The transition from one regime to the other is very abrupt, so that a thermal-to-quantum crossover temperature $T^*$ may be defined by indicating whether nucleation takes place thermally ($T > T^*$) or quantically ($T < T^*$). In the limit of zero temperature, cavitation is purely quantal, but for $T^* > T > 0$ thermally assisted quantum cavitation is the physical process.

For $T < T^*$ the tunnelling rate is

$$J_Q = J_{0Q} \exp(-S^Q/\hbar), \tag{4}$$

where $\mathcal{P} = \exp(-S^Q/\hbar)$ is the tunnelling probability, $S^Q$ is the quantum action, and the prefactor $J_{0Q}$ is again of the order of the number of nucleation sites per unit volume times an attempt frequency $\nu_Q$ which can be estimated from the zero point motion of the system about the metastable equilibrium position $R_{\min}$.

An analytical expression for $T^*$ is obtained which involves the second derivative of $U(R)$ and the value of the collective mass of the bubble $M(R)$ at the maximum of the cavitation barrier, $R_{\max}$

$$k_B T^* = \frac{\hbar}{2\pi} \sqrt{\frac{-1}{M(R_{\max})} \frac{d^2U}{dR^2}\bigg|_{R_{\max}}}. \tag{5}$$

If the motion is irrotational and the fluid incompressible, the collective mass $M$ depends on $R$ as[10,13]

$$M(R) = \frac{4\pi}{\hbar^2} R^3 m_{He} \rho_b, \tag{6}$$

where $\rho_b$ is the particle density of the metastable bulk liquid and $m_{\mathrm{He}}$ is the mass of a helium atom. Eq. (5) shows that the value of $T^*$ is determined by *small variations around* $R_{\max}$. An expression for the attempt frequency in the quantum regime can be also worked out easily:

$$\nu_Q = \frac{1}{2\pi\hbar} \sqrt{\frac{1}{M(R_{\min})} \frac{d^2U}{dR^2}\bigg|_{R_{\min}}}. \tag{7}$$

Using Eq. (5) we have determined $T^*(P)$ and the results are shown in Fig. 2. This figure shows that in the capillary approximation, irrespective of the pressure, above $T \sim 10\,\mathrm{mK}$ the cavitation process is thermal and not quantal. To determine which $T^*$ corresponds to the actual experimental conditions, one has to look for the intersection of the curve $T^*(P)$ with

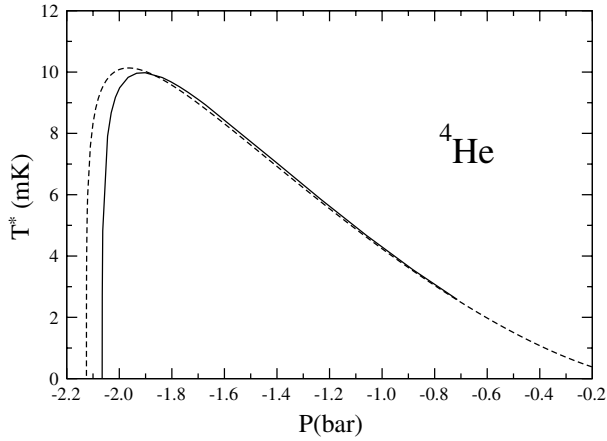


Fig. 2. Crossover temperature $T^*$ (mK) as a function of $P$ (bar) of an electron bubble in liquid $^4$He in the capillary model (dashed line) and in the DF approach (solid line).

the line that results imposing that critical bubbles nucleate with appreciable probability inside the experimental volume during the experimental time:

$$1 = t_{\rm exp} V_{\rm exp} J_{0Q}\, {\rm e}^{-S^Q_{\rm min}/\hbar} = t_{\rm exp} V_{\rm exp} J_{0T}\, {\rm e}^{-\Delta U(P)/k_B T^*}, \tag{8}$$

where $t_{\rm exp}$ and $V_{\rm exp}$ are the experimental time and volume, respectively, and $J_{0Q} = n_e \nu_Q$. Taking[9] $t_{\rm exp} \sim 10^{-5}$ s, $V_{\rm exp} \sim 10^{-5}\,{\rm cm}^3$, $n_e = 10^6\,{\rm cm}^{-3}$, and the value $\nu_Q \sim 10^9\,{\rm s}^{-1}$ obtained from Eq. (7), one gets $T^* = 4.7$ mK at a pressure slightly above $P_u$. At $T^* = 4.7$ mK one has $S^Q = 11.5\,\hbar$, so that the use of the formalism of Ref. 13 is well justified.[17] Had we used the WKB approximation[28] to estimate $T^*$, we would have obtained similar results. In particular, the maximum of $T^*_{WKB}$ is 9.6 mK. We will see in Sec. 3 how these results change in the DF approach.

For a given temperature above $T^*$, the solution to Eq. (8) with $J_T$ instead of $J_Q$ yields the pressure at which critical electron bubbles are created with sizeable probability. For the mentioned experimental parameters, it turns out that in the $T \sim 1$ K regime this happens when $\Delta U \sim 11.5$ K. Inspection of Fig. 1 readily shows that this pressure is very close to $P_u$. Consequently, $P_u$ is the key quantity for electron bubble explosions.[9]

We would like to recall why the capillary model is expected to be fairly realistic for electron bubble explosions whereas it is completely unrealistic to address homogeneous cavitation in liquid helium. Dropping the electron contributions to Eq. (1), it is easy to see that for negative pressures $\Delta U = 16\pi\sigma^3/3|P|^2$ at $R_{\rm max} = 2\sigma/|P|$. This means that the barrier

height is not zero at the spinodal pressure, which is very unphysical. This drawback renders useless the capillary model for homogeneous cavitation in pure liquid helium at low $T$ because it has been experimentally established that cavitation occurs near the spinodal region.[3,4,29]

On the other hand, near $R_{\min}$ the model yields empty bubbles of very small radius, which is also unphysical. As a consequence, any dynamical approach based on the use of these bubble configurations is rather dubious.[30] The model can only work well for large bubbles, as for example near the saturation curve. In these situations, it has been shown that it yields realistic homogeneous cavitation pressures,[1,4,31] and the use of Eq. (5) to obtain $T^*$ yields values in good agreement with the DF ones.[14,32] The situation is quite similar to that found in the description of supersaturated $^3$He–$^4$He liquid mixtures, see Refs. 13 and 33 for a thorough discussion.

## 3. DENSITY-FUNCTIONAL APPROACH TO ELECTRON BUBBLE EXPLOSIONS

Density functional theory has been applied in the past to cavitation in classical liquids (see Ref. 34 and Refs. therein). Since the pioneering work of Xiong and Maxis,[23] it has proven to be the most successful approach in addressing cavitation in liquid helium so far.[14] It incorporates in a self-consistent way the equation of state of bulk liquid and surface tension of the liquid–gas interface as a function of temperature, which are key ingredients of any cavitation model. It does not impose a priori the density profile of the critical cavity, allowing for a flexible description of the process from the saturation line down to the spinodal line. Moreover, within DF theory one avoids to split the system into a bulk and a surface region, and the use of macroscopic concepts such as surface tension and pressure at a nanoscopic scale. However, it is a continuous, not an atomic description of the system. In spite of this, it has been found to well describe situations in which the atomic scale is relevant, such as quantized vortices, or the presence of strongly attractive atomic or molecular impurities (see for instance Ref. 35 and Refs. therein).

In the frame of DF theory, the properties of an electron bubble approaching the surface of liquid $^4$He have been studied by Ancilotto and Toigo.[36] They have used the so-called Orsay-Paris zero temperature finite-range DF,[37] and the pseudopotential proposed in Ref. 38 as e–He interaction. The method chosen by Classen *et al.*[9] is a simplification of that of Ref. 36 in two respects. First, they have used a zero-range DF to describe $^4$He, which seems justified in view of the slowly varying helium densities even in the presence of excess electrons in the liquid (the situation is

completely different for strongly attractive atomic or molecular impurities, see for example Ref. 39). However, they have included some thermal effects in the DF, whereas the approach of Ancilotto and Toigo is at zero temperature.[36] Second, the pseudopotential has been replaced by a contact e–He interaction whose intensity has been adjusted so as to reproduce the total energy of an excess electron in bulk helium,[40] which is about 1 eV for a particle density of $0.0218\,\text{Å}^{-3}$ (saturation density).

Our starting point is a finite temperature zero-range DF that reproduces thermal properties of liquid $^4$He such as the experimental isotherms and the $^4$He liquid–gas coexistence line up to $T = 4.5\,\text{K}$, and the $T$ dependence of the surface tension of the liquid free surface.[21] This DF has been successfully used to address homogeneous cavitation in liquid helium from $T \sim 0\,\text{K}$ up to temperatures close to the critical one.[4] In the quantum cavitation regime, it has also yielded results in good agreement with experiment[3] and with other theoretical approaches.[41] We have taken the Hartree-type e–He effective potential derived by Cheng *et al.*[42] (see also Ref. 18) as e–He interaction. This allows us to write the free energy of the system as a functional of the $^4$He particle density $\rho$, the excess electron wave function $\Psi$ and $T$:

$$F[\rho, \Psi, T] = \int d\vec{r}\, f(\rho, T) + \frac{\hbar^2}{2m_e} \int d\vec{r} |\nabla \Psi(\vec{r})|^2 + \int d\vec{r} |\Psi(\vec{r})|^2 V(\rho), \quad (9)$$

where $f(\rho, T)$ is the $^4$He free energy density per unit volume written as

$$f(\rho, T) = f_{\text{vol}}(\rho, T) + \beta \frac{(\nabla \rho)^2}{\rho} + \xi (\nabla \rho)^2. \quad (10)$$

In this expression, $f_{\text{vol}}(\rho, T)$ consists of the well-known free energy density of a Bose gas, plus phenomenological density dependent terms that take into account the effective interaction of helium atoms in the bulk liquid.[21] The parameters of these terms and those of the density gradient terms in Eq. (10) have been adjusted so as to reproduce physical quantities such as the equation of state of the bulk liquid and the surface tension of the liquid free surface. We have slightly modified the original value[21] of the parameter $\xi$ in Eq. (10) to exactly reproduce the surface tension of liquid $^4$He (Ref. 19), taking $\xi = 2330\,\text{K}\,\text{Å}^5$. The $\beta$-term is a kinetic energy term; at $T = 0$ the system is described as a Bose condensate and for this reason the kinetic energy arises only from the inhomogeneity of the density.[43] For inhomogeneous systems, this term is essential to have densities well behaved everywhere, and in the case of $^4$He droplets its inclusion in the functional yields densities that smoothly-exponentially-go from the bulk liquid down to zero. We have taken[43] $\beta = (\hbar^2/2m_4)/4$.

In bulk helium, knowledge of $f(\rho, T)$ enables solution of the phase equilibrium equations and to determine the spinodal line. It also yields an equation of state in the negative pressure regime, inaccessible to the experimental determination, through the thermodynamic relationship $P = -f_{\text{vol}}(\rho, T) + \mu\rho$, where $\mu$ is the $^4$He chemical potential.

The e–He interaction $V(\rho)$ is written as a function of the local helium density[42]

$$V(\rho) = \frac{\hbar^2 k_0^2}{2m_e} + \frac{2\pi\hbar^2}{m_e}\rho a_\alpha - 2\pi\alpha e^2 \left(\frac{4\pi}{3}\right)^{1/3} \rho^{4/3}, \tag{11}$$

where $\alpha = 0.208\,\text{Å}^3$ is the static polarizability of a $^4$He atom, and $k_0$ is determined from the helium local Wigner–Seitz radius $r_s = (3/4\pi\rho)^{1/3}$ by solving the transcendent equation

$$\tan[k_0(r_s - a_c)] = k_0 r_s \tag{12}$$

with $a_c$ and $a_\alpha$ being the scattering lengths arising from a hard-core and from a polarization potential. We have taken[42] $a_\alpha = -0.06\,\text{Å}$, $a_c = 0.68\,\text{Å}$.

The application of DF theory to the cavitation problem proceeds as follows. For given $P$ and $T$ values one first determines the metastable and unstable cavities that would correspond to the local minimum and maximum configurations in the capillary model (actually, in the multidimensional space spanned by the more flexible DF configurations, the latter is no longer a local maximum but a saddle point). This is achieved by solving the Euler–Lagrange equations which result from the variation of the constrained grand potential density $\tilde{\omega}(\rho, \Psi, T) = \omega(\rho, \Psi, T) - \varepsilon|\Psi|^2$, where the grand potential density $\omega(\rho, \Psi, T)$ is defined from Eq. (9) as

$$\omega(\rho, \Psi, T) = f(\rho, T) + \frac{\hbar^2}{2m_e}|\nabla\Psi|^2 + |\Psi|^2 V(\rho) - \mu\rho. \tag{13}$$

It yields

$$\frac{\delta f}{\delta\rho} + |\Psi|^2 \frac{\partial V}{\partial\rho} = \mu, \tag{14}$$

$$-\frac{\hbar^2}{2m_e}\Delta\Psi + V(\rho)\Psi = \varepsilon\Psi, \tag{15}$$

where $\varepsilon$ is the lowest eigenvalue of the Schrödinger equation obeyed by the electron. These equations are solved assuming spherical symmetry, imposing for $\rho$ the physical conditions that $\rho'(0) = 0$ and $\rho(r \to \infty) = \rho_b$, where $\rho_b$ is the density of the metastable bulk liquid, and that the electron is in the $1s$ state. Fixing $\rho_b$ and $T$ amounts to fix $P$ and $T$, as the pressure can be obtained from the bulk equation of state $P = -f_{\text{vol}}(\rho_b, T) + \mu\rho_b$ as

well as $\mu$. Thus, $\mu = \partial f_{\rm vol}(\rho, T)/\partial\rho|_T$ is known in advance, whereas $\varepsilon$ is not and has to be determined from Eq. (15).

We have solved Eqs. (14) and (15) using a multidimensional Newton–Raphson method[44] after having discretized them using $n$-point formulas for the $r$ derivatives. We have used $n = 13$ formulas, but comparable results have been obtained using $n = 7$ and 9 formulas.[45] A fine mesh of step $\Delta r = 0.1$ Å has been employed, and the equations have been integrated up to $R_\infty = 150$ Å to make sure that the asymptotic bulk liquid has been reached. The multidimensional Newton–Raphson method has been applied until the *local chemical potential*-left hand side of Eq. (14)–does not differ substantially from $\mu$. We have checked that, for every $r$ value, both coincide up to at least the sixth decimal figure. This is a crucial test on the accuracy of our method. We have thus achieved a *fully variational solution* of the Euler–Lagrange problem embodied in Eqs. (14) and (15), valid from $r = 0$ up to $R_\infty$.

We represent in Fig. 3 several $^4$He density profiles and excess electron squared wave functions $|\Psi|^2$. The top panel shows the stable bubble at $T = 0$ K, $P = 0$ bar. The other three panels display the near-to-unstable electron bubble for several $(P, T)$ values. For a given $T$, they have been obtained decreasing $\rho_b$, i.e. $P$, until Eqs. (14) and (15) have no solution. The smaller $P$ value defines $P_u$. The $^4$He instability pressure $P_u$ is shown in Fig. 4 as a function of $T$. This figure shows that the lowest pressure the system may reach before becoming macroscopically unstable is $P_u = -2.07$ bar, which is the value corresponding to $T = 0$ K.

As we have indicated, in the metastability region the Euler–Lagrange equations have two different solutions for given $\rho_b$ and $T$-i.e., $P$ and $T$-values, one corresponding to the metastable configuration and another corresponding to the saddle configuration. A similar situation is found in the case of cavitation in the presence of vortices.[46] Actually, it is the search of the saddle configuration that constitutes a numerical challenge. The reason is that, due to the strongly repulsive e–He interaction, fairly small changes in the electron configuration induce changes in the helium configuration hard to handle numerically, so that in the course of the numerical procedure, the system has a strong tendency to jump from the saddle to the metastable solution. We have represented in Fig. 5 several $^4$He density profiles and excess electron squared wave functions $|\Psi|^2$ corresponding to the metastable and saddle electron bubbles for $T = 0$, 2 and 4 K, and a value of $P$ close to $P_u$.

The cavitation barrier height $\Delta\Omega_{\rm max}$ is obtained by subtracting the grand potential of the saddle bubble $\omega(\rho_s, \Psi_s, T)$ from that of the metastable bubble $\omega(\rho_m, \Psi_m, T)$:

$$\Delta\Omega_{\rm max} = \int d\vec{r}[\omega(\rho_s, \Psi_s, T) - \omega(\rho_m, \Psi_m, T)]. \tag{16}$$

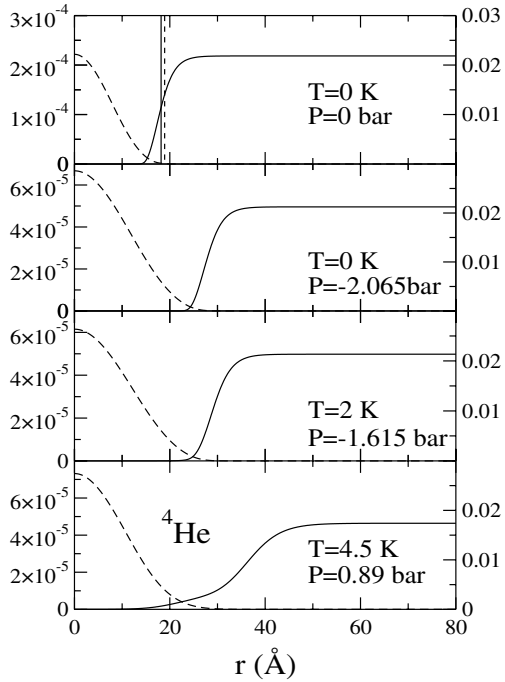


Fig. 3. $^4$He density profiles in Å$^{-3}$ (solid lines, right scale) and excess electron squared wave functions $|\Psi|^2$ in Å$^{-3}$ (dashed lines, left scale), as a function of radial distance $r$ (Å). The top panel shows the stable bubble at $T=0$ K, $P=0$ bar. The other three panels show the near-to- unstable electron bubble for several $(P,T)$ values. In the upper panel, the vertical thin dashed line indicates the radius of the capillary model bubble ($R_{\min}=18.9$ Å), and the vertical thin solid line indicates the radius at which the helium density equals $\rho_b/2[R(\rho_b/2)=18.0$ Å, with $\rho_b=0.0218$ Å$^{-3}$].

Since both configurations go asymptotically to the same $\rho_b$ value, Eq. (16) gives $\Delta\Omega_{\max}$ as a function of $P$ and $T$ via the equation of state of bulk liquid helium. $\Delta\Omega_{\max}$ is shown in Fig. 6 as a function of $P$ for $T=2$ and 4 K, and in Fig. 1 for $T=0$ K. As indicated, $\Delta\Omega_{\max}$ becomes negligible when the system approaches the unstability pressure. This constitutes a suplementary test on the correctness of the near-to-unstable configurations we have found by decreasing $\rho_b$ at fixed $T$. Otherwise, $\Delta\Omega_{\max}$ would not be negligible for this configuration.

Once $\Delta\Omega_{\max}(P,T)$ has been determined, it can be used to obtain the critical pressure $P_{\rm cr}$ at which critical bubbles nucleate at an appreciable rate by solving an equation similar to Eq. (8):

$$1=t_{\exp}V_{\exp}J_{0T}\,\mathrm{e}^{\Delta\Omega_{\max}(P,T)/k_BT} \tag{17}$$

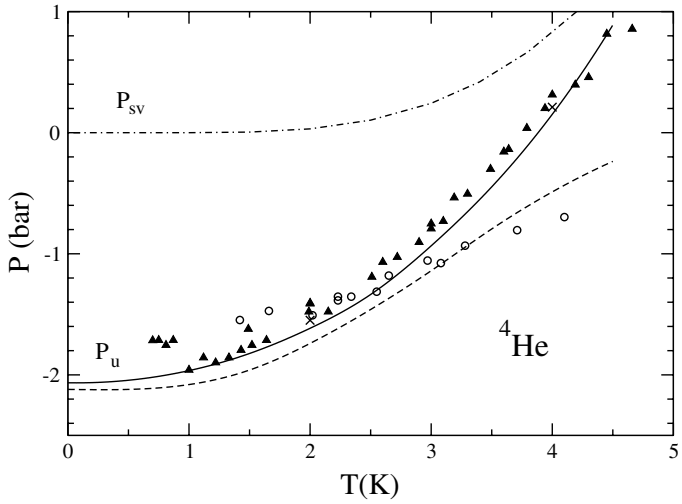


Fig. 4. Instability pressure $P_u$ as a function of $T$ for $^4$He. Circles and triangles are experimental data from Refs. 8 and 9, respectively. The results of the capillary model are represented by a dashed line, and the DF results by a solid line. The dash-dotted line represents the experimental saturation vapor pressure $P_{sv}$ line. The crosses at $T = 2$ and 4 K indicate the critical pressures $P_{cr}$.

taking $J_{0T} = v_T n_e$. This yields $P_{cr} = -1.55$ bar at $T = 2$ K, and $P_{cr} = 0.211$ bar at $T = 4$ K. These pressures are slightly above the corresponding $P_u$ values which are, respectively, $-1.62$ and 0.151 bar.

We thus see from Fig. 4 that our results are fully compatible with the available experimental data—the calculated $P_u$ should be a lower bound to the cavitation pressure—if the experimental results of Ref. 8 are ruled out, and those carried out more recently by the same group[9] have error bars similar to those found in the case of pure liquid $^4$He,[29] as well as in the case of electron bubble cavitation in $^3$He.[10]

The capillary model yields instability pressures lower than those obtained within DF theory, especially at high-temperatures. The discrepancy arises even if one takes into account, as we did, the $T$-dependence of the surface tension. The origin of the discrepancy is the e–He strongly repulsive interation acting on the helium density tail that penetrates inside the cavity as $T$ increases: the electron has to 'push' not only the bulk surface, which for DF configurations is at the radius where the helium density equals $\rho_{b/2}$, but also the part of the helium density that is spread inside the bubble, especially at high temperatures. This 'pushing' produces a steeper bubble density profile, and not only an actual displacement of

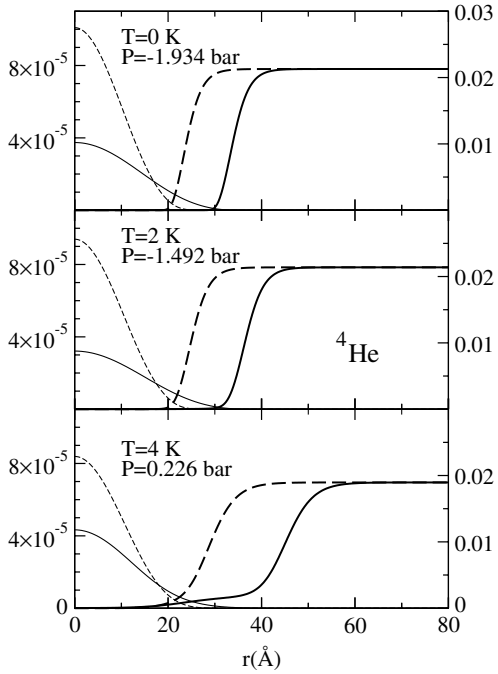


Fig. 5. $^4$He density profiles in Å$^{-3}$ (thick lines, right scale) and excess electron squared wave functions $|\Psi|^2$ in Å$^{-3}$ (thin lines, left scale), as a function of radial distance $r$ (Å) for the metastable and saddle electron bubble at different $(P, T)$ values. Dashed lines correspond to the metastable configuration, and solid lines to the saddle configuration. From top to bottom, the $\Delta\Omega_{\max}$ values are 65.3, 80.2, and 88.1 K, respectively.

its surface. For this reason, the radius of the bubbles are smaller in the DF than in the simple capillary approach (see Figs. 3 and 8). Part of the difference is removed if one allows for penetration of the electron wave function into the liquid using a finite height barrier for the potential that confines the electron within the bubble. This would diminish the bubble radius, as it lowers the zero-point energy of the electron. However, the final effect is that it increases $|P_u|$ and the agreement with the DF result worsens.[9]

Our results for $P_u$ are slightly below those of Ref. 9 (compare for instance our value of $-2.07$ bar at $T = 0$ K with their value of $-1.92$ bar). This difference is essentially due to the different value of the surface tensions used to build the DF used in our work and in theirs. Indeed, the pressure we obtain if the DF is adjusted to reproduce the surface tension of Ref. 20 is $P_u = -1.93$ bar, in excellent agreement with the value

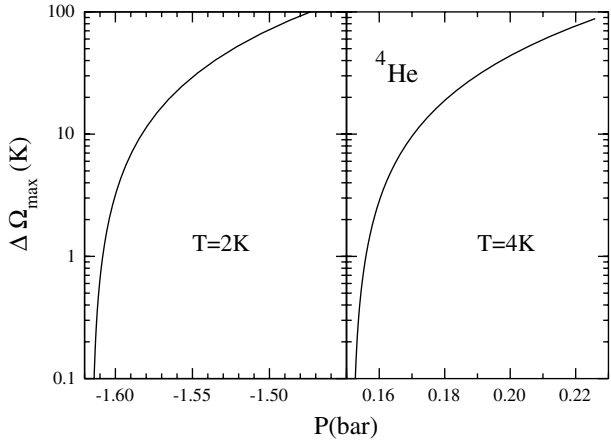


Fig. 6. DF energy barrier height $\Delta\Omega_{\max}$ (K) for $^4$He as a function of $P$ (bar) for $T = 2\,\mathrm{K}$ (left panel) and $T = 4\,\mathrm{K}$ (right panel).

found in Ref. 9. Moreover, the ratio 2.07/1.93 compares very well with that obtained from Eq. (2) if ones takes $\sigma = 0.272\,\mathrm{K\,\AA^{-2}}$ in one case, and $\sigma = 0.257\,\mathrm{K\,\AA^{-2}}$ in the other. We recall that in Ref. 9 the kinetic $\beta$-term in Eq. (10) has been neglected, which makes the helium density to be zero at the origin, and that these authors have made the helium density strictly zero inside a sphere around the excess electron, whereas in our case the helium density is defined everywhere. These differences do not seem to play any role.

We have also obtained $\Delta\Omega_{\max}$ at $T = 0\,\mathrm{K}$ using the contact e–He interaction used in Ref. 9. The results, indicated by crosses in Fig. 1, indicate that the contact interaction sensibly yields the same barrier heights as the Hartree-type interaction.

We have employed the DF theory to obtain the crossover temperature $T^*$.[47] To this end, one has to obtain the frequency of the small amplitude oscillations around the saddle configuration in the inverted barrier potential well. From the capillary model results we expect that $T^*$ is very small, so that thermal effects on $\rho_s$ can be neglected. In view of the fairly large size of the saddle bubble, the oscillation frequency can be obtained as follows.[32,48] After determining the saddle configuration $\rho_s(r)$, we define a continuous set of densities by a rigid translation of $\rho_s(r)$:

$$\rho_\delta(r) \equiv \begin{cases} \rho_s(r=0) & \text{if } r \leqslant \delta, \\ \rho_s(r-\delta) & \text{if } r \geqslant \delta. \end{cases} \tag{18}$$

The variable $\delta$ roughly represents the displacement of the surface of the saddle configuration with respect to its stationary value. Varying $\delta$, all physically relevant configurations are generated. Eq. (18) implies that the surface diffuseness of the bubble is kept frozen during the displacement.

The barrier is then obtained as a function of $\delta$:

$$\Delta\Omega_\delta = \int d\vec{r}[\omega(\rho_\delta, \Psi_\delta, T=0) - \omega(\rho_m, \Psi_m, T=0)]. \tag{19}$$

Within this model, $\delta$ is the only collective variable describing the bubble oscillation, and all the time-dependence is in $\delta(t)$. The kinetic energy associated with the oscillation is

$$E_{\text{kin}} = \frac{m_{\text{He}}}{2} \int d\vec{r}\, \rho(\vec{r}, t)\, \vec{u}^2(\vec{r}, t), \tag{20}$$

where $\vec{u}(\vec{r}, t)$ is the velocity field which can be formally obtained from the continuity equation

$$\frac{\partial \rho}{\partial t} + \vec{\nabla}(\rho \vec{u}) = 0. \tag{21}$$

It yields:

$$u(r, t) = -\frac{1}{r^2 \rho(r, t)} \int_0^r s^2 \dot{\rho}(s, t) ds. \tag{22}$$

By construction,

$$\rho(r, t) = \rho_s(r - \delta(t)). \tag{23}$$

Thus

$$\dot{\rho}(r, t) = -\rho_\delta'(r)\dot{\delta} \tag{24}$$

and

$$u(r, t) = \frac{\dot{\delta}}{r^2 \rho_\delta(r)} \left[ r^2 \rho_\delta(r) - 2 \int_0^r s \rho_\delta(s) ds \right]. \tag{25}$$

Defining the mass parameter M($\delta$) as

$$E_{\text{kin}} \equiv \frac{\hbar^2}{2} M(\delta) \dot{\delta}^2, \tag{26}$$

we get

$$M(\delta) = \frac{4\pi m_{\text{He}}}{\hbar^2} \int_0^\infty \frac{\mathrm{d}r}{r^2 \rho_\delta(r)} \left[ r^2 \rho_\delta(r) - 2 \int_0^r ds\, s \rho_\delta(s) \right]^2. \tag{27}$$

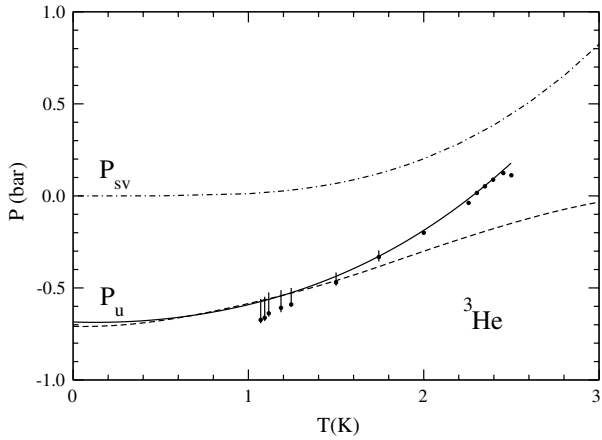


Fig. 7. $^3$He instability pressure $P_u$ as a function of $T$. Dots are experimental data from Ref. 10. The dash-dotted line represents the experimental saturation vapor pressure $P_{sv}$ line. The results of the capillary model are represented by a dashed line, and the DF results by a solid line.

Proceeding as in the capillary case one obtains

$$k_B T^* = \frac{\hbar}{2\pi} \sqrt{-\frac{\partial^2 \Delta\Omega}{\partial \delta^2} / M(\delta)\Big|_{\delta=0}}, \tag{28}$$

which is the generalization of Eq. (5) to the case of diffuse density profiles. Using this equation we have obtained the $T^*(P)$ curve shown in Fig. 2, and proceeding as in the capillary model, we have determined a crossover temperature of 6.0 mK.

## 4. ELECTRON BUBBLE EXPLOSIONS IN LIQUID $^3$HE

We have also studied the explosion of electron bubbles in the case of liquid $^3$He. The capillary model of Sec. 2 can be straightfowardly applied to this isotope using the appropriate values of the surface tension $\sigma = 0.113\,\mathrm{K\,\AA^{-2}}$ (Ref. 49, where one may also find the values of $\sigma(T)$ we have used to obtain the capillary model results we show in Fig. 7) and of the dielectric constant $\epsilon = 1.0428$ (Ref. 50) As in Sec. 2, we have neglected this term in the calculations because of its smallness.

At zero pressure and temperature, the capillary model yields an electron bubble of radius $R_{\min} = 23.5\,\mathrm{\AA}$, larger than for $^4$He because of the smaller $^3$He surface tension. For the same reason, the $^3$He instability pressure $P_u = -0.71$ bar is smaller in absolute value [see Eq. (2)]. This pressure is atteined for an electron bubble of radius $R_u = 35.2\,\mathrm{\AA}$.

The application of DF theory to describe electron bubble explosions in $^3$He proceeds as indicated in Sec. 3. We have used the functional proposed in Ref. 51 which we have employed in the past[25] to describe homogeneous cavitation in liquid $^3$He, and the e–He interaction given in Eq. (11) with the parameters corresponding to $^3$He, namely $\alpha = 0.206\,\text{Å}^3$, and same values for $a_\alpha$ and $a_c$.

The $^3$He instability pressure $P_u$ is shown in Fig. 7 as a function of $T$. This figure shows that the lowest pressure the system may reach before becoming macroscopically unstable is $P_u = -0.69$ bar, which is again the value corresponding to $T = 0\,\text{K}$. For the reason indicated before, we have not considered necessary to calculate the critical pressures in the case of $^3$He. It can be seen that our values of $P_u$ are somewhat above the experimental values of $P_{\text{cr}}$ obtained in Ref. 10, especially at $T \sim 1\,\text{K}$. As in the $^4$He case, the capillary model fails as soon as thermal effects start being sizeable.

We represent in Fig. 8 several $^3$He density profiles and excess electron squared wave functions $|\Psi|^2$. The top panel shows the stable bubble at $T = 0\,\text{K}$, $P = 0$ bar. The other three panels display the near-to-unstable electron bubble for several $(P, T)$ values. Comparing with Fig. 3, it can be seen that $^3$He electron bubbles are more diffuse than $^4$He electron bubbles.

We have also obtained $T^*$ for $^3$He in the capillary model. In spite of theoretical predictions that point to a crossover temperature of the order of 100 mK in pure liquid $^3$He,[41,47] recent experiments have not found such a crossing,[52] indicating that superfluid coherence might play a role in quantum cavitation. Yet, using the expressions given in Sec. 2 we have obtained $T^*(P)$ for $^3$He and show it in Fig. 9. It can be seen that the maximum of $T^*(P)$ is roughly half the value we have obtained for $^4$He in the capillary model. Proceeding as in the case of $^4$He and assuming the same experimental parameteres, we have found that the value of $T^*$ that would correspond to this situation is about 2.3 mK. This estimate is close to the normal-to-superfluid transition temperature in $^3$He, below which our DF method does not apply as it assumes that $^3$He is in the normal phase.

## 5. SUMMARY

We have thoroughly addressed electron bubble explosions in liquid helium. Our approach is based on the application of finite temperature density functionals succesfully used to describe cavitation in liquid $^4$He and $^3$He. This approach is fully selfconsistent and unbiased by numerical aitifacts, and to our knowledge, it is the only one applied in a wide range of temperatures.

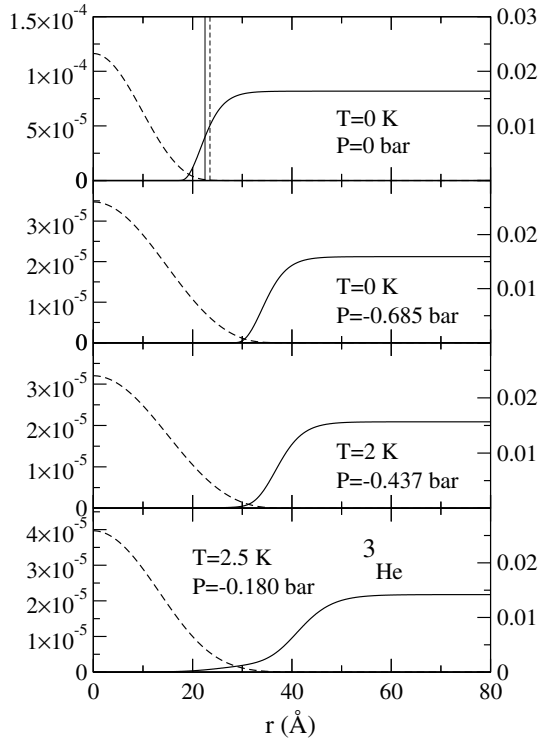


Fig. 8. $^3$He density profiles in Å$^{-3}$ (solid lines, right scale) and excess electron squared wave functions $|\Psi|^2$ in Å$^{-3}$ (dashed lines, left scale), as a function of radial distance $r$ (Å). The top panel shows the stable bubble at $T = 0\,\mathrm{K}$, $P = 0\,\mathrm{bar}$. The other three panels show the near-to-unstable electron bubble for several $(P, T)$ values. In the upper panel, the vertical thin dashed line indicates the radius of the capillary model bubble ($R_{\min} = 23.5\,$Å), and the vertical thin solid line indicates the radius at which the helium density equals $\rho_b/2[R(\rho_b/2) = 22.5$ Å, with $\rho_b = 0.0163\,\mathrm{Å}^{-3}$].

We have compared our results with experiments and have found that our calculations are either in agreement with the experimental data,[9,10] or compatible with them if they have error bars similar to these attributed to other cavitation processes in liquid helium.

We have used a realistic electron–helium interaction and have tested another approach based on the use of a simpler interaction. We have found that in spite of the fairly large electron bubbles involved in the process, at high temperatures the capillary model fails to yield quantitative results, overestimating the critical pressures. We attribute this to the 'rigidity' of the bubble configurations which is inherent to the capillary

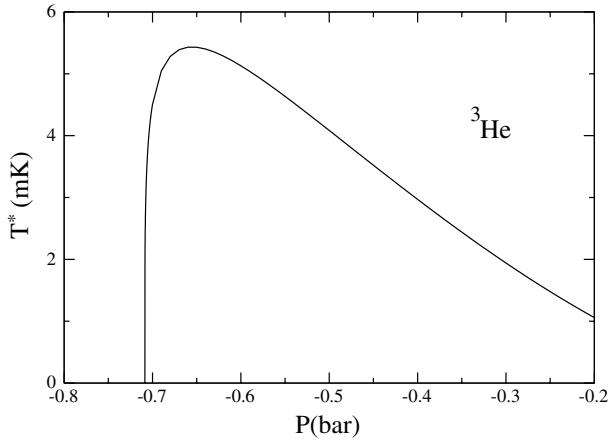


Fig. 9. Crossover temperature $T^*$(mK) as a function of $P$ (bar) of an electron bubble in liquid $^3$He in the capillary model.

approach. Whereas these are serious drawbacks for nanoscopic bubbles, they are expected not to have a sizeable influence for microscopic multi-electron bubbles.[53]

We have also used the density functional results in conjunction with a functional integral method to obtain the thermal to quantum crossover temperature. This approach has led in the past to a correct description of the same process in pure liquid $^4$He. In the present case, the crossover temperature turns out to be very small, about 6 mK.

Finally, we want to stress the suitability of the DF approach to quantitatively address electron bubbles in liquid He. This might encourage one to investigate other problems like the infrared spectrum of the electron bubble in liquid helium, and the effect of quantized vortices pinned to excess electrons on the critical cavitation pressure. It has been argued[54] hat the rising of $P_u$ below $T = 1$ K could be attributed to the presence of quantized vortices. However, only simple models have been used to study their effect, and the agreement with experiment is only qualitative. In the case of the infrared spectrum of electron bubbles, the DF approach might shed light on the long-standing problem of how to understand the experimental results of Grimes and Adams[55] on the $1s - 1p$ and $1s - 2p$ electron transition energies without using unjustifiable pressure dependences of the helium surface tension within the capillary model.

## ACKNOWLEDGMENTS

We would like to thank F. Ancilotto, F. Caupin, M. Guilleumas, D. M. Jezek, H. Maris and F. Toigo for useful discussions. This work has been performed under grants BFM2002-01868 from DGI (Spain) and 2000SGR00024 from Generalitat de Catalunya.

## REFERENCES

1. J. A. Nissen, E. Bodegom, L. C. Brodie, and J. Semura, *Phys. Rev. B* **40**, 617 (1989).
2. Q. Xiong and H. J. Maris, *J. Low Temp. Phys*. **82**, 105 (1991).
3. H. Lambaré, P. Roche, S. Balibar, H. J. Maris, O. A. Andreeva, C. Guthmann, K. O. Keshishev, and E. Rolley, *Eur. Phys. J. B* **2**, 381 (1998).
4. S. Balibar, *J. Low Temp. Phys*. **129**, 363 (2002).
5. T. Satoh, M. Morishita, M. Ogata and S. Katoh, *Phys. Rev. Lett*. **69**, 335 (1992).
6. S. Balibar, C. Guthmann, H. Lambaré, P. Roche, E. Rolley, and H. J. Maris, *J. Low Temp. Phys*. **101**, 271 (1995).
7. X. Chavanne, S. Balibar, and F. Caupin, *J. Low Temp. Phys*. **126**, 615 (2002).
8. J. Classen, C.-K. Su, and H. J. Maris, *Phys. Rev. Lett*. **77**, 2006 (1996).
9. J. Classen, C.-K. Su, M. Mohazzab, and H. J. Maris, *Phys. Rev. B* **57**, 3000 (1998).
10. C.-K. Su, C. E. Cramer, and H. J. Maris, *J. Low Temp. Phys*. **113**, 479 (1998).
11. F. Dalfovo, *Phys. Rev. B* **46**, 5482 (1992).
12. H. J. Maris, *J. Low Temp. Phys*. **94**, 125 (1994).
13. M. Barranco, M. Guilleumas, D. M. Jezek, R. J. Lombard, J. Navarro, and M. Pi, *J. Low Temp. Phys*. **117**, 81 (1999).
14. M. Barranco, M. Guilleumas, M. Pi, and D. M. Jezek, in *Microscopic Approaches to Quantum Liquids in Confined Geometries,* E. Krotscheck and J. Navarro eds. p. 319 World Scientific, Singapore (2002).
15. M. Pi, M. Barranco, and R. Mayol, contribution to the Symposium on Quantum Fluids and Solids, Trento (Italy), July 5–9, 2004. *J. of Low Temp. Phys*. **138**, 463 (2005). Due to an unfortunate mistake in the electron–helium interaction energy, the numerical results presented in this reference are in error.
16. R. A. Ferrel, *Phys. Rev*. **108**, 167 (1957).
17. D. Konstantinov and H. J. Maris, *J. Low Temp. Phys*. **121**, 609 (2000).
18. M. Rosenblit and J. Jortner, *Phys. Rev. B* **52**, 17461 (1995).
19. P. Roche, G. Deville, N. J. Appleyard, and F. I. B. Williams, *J. Low Temp. Phys*. **106**, 565 (1997).
20. M. Iino, M. Suzuki, and A. J. Ikushima, *J. Low Temp. Phys*. **61**, 155 (1985).
21. A. Guirao, M. Centelles, M. Barranco, M. Pi, A. Polls, and X. Viñas, *J. Phys. Condens. Matter* **4**, 667 (1992).
22. H. M. Guo, D. O. Edwards, R. E. Sarwinski, and J. T. Tough, *Phys. Rev. Lett*. **27**, 1259 (1971).
23. Q. Xiong and H. J. Maris, *J. Low Temp. Phys*. **77**, 347 (1989).
24. J. Boronat, J. Casulleras, and J. Navarro, *Phys. Rev. B* **50**, 3427 (1994).
25. D. M. Jezek, M. Guilleumas, M. Pi, A Barranco, and J. Navarro, *Phys. Rev. B* **48**, 16 582 (1993).
26. S. Coleman, *Phys. Rev. D* **15**, 2929 (1977); C. G. Callan and S. Coleman, *ibid*. **16**, 1762 (1977).
27. E. M. Chudnovsky, *Phys. Rev. A* **46**, 8011 (1992).
28. C.-K. Su and H. J. Maris, *J. Low Temp. Phys*. **110**, 485 (1998).
29. F. Caupin and S. Balibar, *Phys. Rev. B* **64**, 064507 (2001).
30. T. Nakamura, Y. Kanno, and S. Takagi, *Phys. Rev. B* **51**, 8446 (1995).
31. D. N. Sinha, J. S. Semura, and L. C. Brodie, *Phys. Rev. A* **26**, 1048 (1982).

32. M. Guilleumas, M. Barranco, D. M. Jezek, R. J. Lombard, and M. Pi, *Czech. J. Phys*. **46**, Suppl. S1, 389 (1996).
33. E. Tanaka, K. Hatakeyama, S. Noma, S. N. Burmistrov, and T. Satoh, *J. Low Temp. Phys*. **127**, 81 (2002).
34. D. W. Oxtoby, *J. Phys. Condens. Matter* **4**, 7627 (1992).
35. F. Ancilotto, M. Barranco, and M. Pi, *Phys. Rev. Lett*. **91**, 105302 (2003).
36. F. Ancilotto and F. Toigo, *Phys. Rev. B* **50**, 12 820 (1994).
37. J. Dupont-Roc, M. Himbert, N. Pavloff, and J. Treiner, *J. Low Temp. Phys*. **81**, 31 (1990).
38. N. R. Kestner, J. Jortner, M. H. Cohen, and S. A. Rice, *Phys. Rev*. **140**, A56 (1965).
39. F. Dalfovo, *Z. Phys. D* **29**, 61 (1994).
40. W. T. Sommer, *Phys. Rev. Lett*. **12**, 271 (1964); M. A. Woolf and G. W. Rayfield, *ibid*. **15**, 235 (1965).
41. H. J. Maris, *J. Low Temp. Phys.* **98**, 403 (1995).
42. E. Cheng, M. W. Cole, and M. H. Cohen, *Phys. Rev. B* 50, 1136 (1994); Erratum *ibid*. 50, 16 134 (1994).
43. S. Stringari and J. Treiner, *J. Chem. Phys*. **87**, 5021 (1987); *Phys. Rev. B* **36**, 8369 (1987).
44. W. H. Press, S. A. Teulosky, W. T. Vetterling, and B. P. Flannery, *Numerical Recipes in Fortran 77: The, Art of Scientific Computing* (Cambridge University Press, Cambridge, 1999).
45. W.G. Bickley, *Math. Gaz*. **25**, 19 (1941); M. Abramowitz and I. A. Stegun, *Handbook of Mathematical Functions* Dover, New York, (1965).
46. D. M. Jezek, M. Guilleumas, M. Pi, and M. Barranco, *Phys. Rev. B* **55**, 11092 (1997).
47. M. Guilleumas, M. Barranco, D. M. Jezek, R. J. Lombard, and M. Pi, *Phys. Rev. B* **55**, 11092 (1997).
48. M. Guilleumas, Ph. D. Thesis, University of Barcelona (1995), unpublished.
49. M. Iino, M. Suzuki, A. J. Ikushima, and Y. Okuda, *J. Low Temp. Phys*. **59**, 291 (1985).
50. M. Rosenblit and J. Jortner, *Phys. Rev. Lett*. **75**, 4079 (1995).
51. M. Barranco, M. Pi, A. Polls, and X. Viñas, *J. Low Temp. Phys*. **80**, 77 (1990).
52. F. Caupin, S. Balibar, and H. J. Maris, *J. Low Temp. Phys*. **126**, 91 (2002).
53. J. Tempere, I. F. Silvera, and J. T. Devreese, *Phys. Rev. B* **67**, 035402 (2003).
54. J. Classen, C.-K. Su, M. Mohazzab, and H. J. Maris, *J. Low Temp. Phys*. **110**, 431 (1998).
55. C. C. Grimes and G. Adams, *Phys. Rev. B* **41**, 6366 (1990).